Proposal of Hybrid Si-Gas Pixel Detector (HSiGPD)

G. Bashindzhagyan, N. Korotkova, A. Romaniouk, N. Sinev and V. Tikhomirov

Abstract

This document is aimed to describe a possibility of a development of a new type of detectors based on merging micro-pattern gaseous detector technology and a new trend in the development of semiconductor detectors. This type of the detectors would offer superior tracking functions, which apart of high precision space point could also provide a track segment reconstructed on-line on a front-end level already for one layer of the detector. These detectors will have self-triggering properties, which can be used as a first level trigger in the particle physics experiments and other applications. In Section 1 main properties of the Gas Pixel detector as a tracking device, which have track segment reconstruction features, are described. Section 2 is dedicated to a description of the algorithm of the on-line track segment reconstruction and the results of simulation. In Section 3 some general design considerations of the hybrid Si-Gas Pixel detector are presented. Detailed description of the electronics modules of the read-out chips including analysis blocks a described in Section 4.

1. Introduction

One of the new promising technologies which can be an alternative to the semiconductor detectors is based on the recent developments of Gas Pixel detectors (GPD) [1-7], see also a PDG review [8]. These detectors can combine the best properties of silicon and gaseous detectors, providing high precision 3D track segments in a single detector layer. Operation principle of these detectors is similar to that of Time Projection Chambers (see, e.g., [9] and references within) with a two-dimensional readout plane. Schematic view of the Gas Pixel detector is shown in Fig. 1. A specially treated pixel electronics chip is placed in the gas volume. The gas volume has a drift gap (width of the gap depends on exact detector requirements) and an electron multiplication region. Detectors might be based on a GEM [1] technology or on a micromegas technology as it shown in Fig. 1 [2-7], The micromegas based detectors have a planar region with high electric filed approximately of 50 μm wide, separated from the drift volume by a mesh or a grid. Primary ionization electrons, produced by a charged particle, drift towards the pixel chip, focused into the grid holes (as it shown in Fig. 1), multiplied between the grid and pixel sensor and are measured by the pixels of the chip. The position of the hit pixel gives two coordinates in the pixel plane, while the measured drift time gives a third coordinate of a primary ionization. Depending on the exact realization of the chip functionality it is possible to measure time or amplitude or both simultaneously if required. The charged particle track can be reconstructed from the measured ionization points, giving a precise measurement of a space point (the point where the particle crosses the pixel chip plane), the angle in the chip plane, and the angle of incidence to the chip plane (3D track segment).

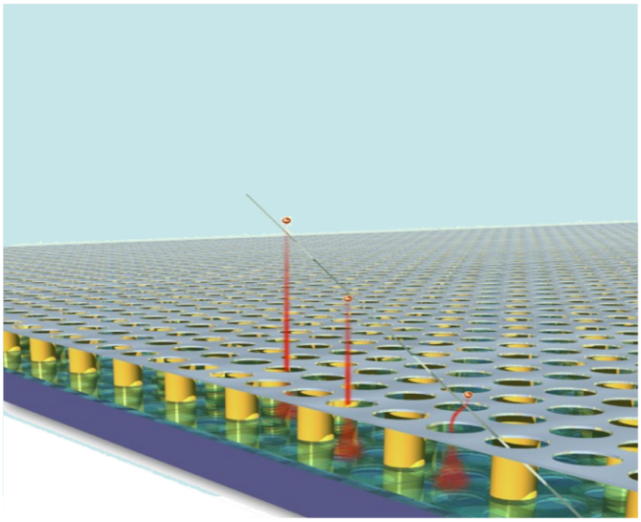

Figure 1. Schematic view of the Gas Pixel detector. The pixel chip is separated from a drift volume by a mesh. Electron amplification happens in the gap between the mash and the pixel chip.

Possibility to reconstruct 3D track segments has two important applications for tracking detectors. Usually tracking systems in most of experiments contain quite a few layers of the detectors, which measure space points (hits) on a particle track. At high particle track density many hit combinations are considered and finally all ambiguities are removed by iterative process of a track fitting. New technology allows to provide not only a precise space point but using a tack segment in one detector layer but it can also predict a space point in the next layer of the tracking system, significantly reducing the number of combinations, and hence track reconstruction processing time (``vector'' tracking). The second application is based on a specific feature of these detectors. When a particle traverses a gaseous volume it produces many ionization clusters. Diffusion makes drifting electrons to be collected by different pixels. In experiments operating at high trigger rate the amount of the information being sent to back-end electronics is too large and data must be compressed already at the front-end level. This means that basic data processing must be performed already on chip level, sending out only the track spatial coordinates and two angles. This processing can be carried out in a few tens of clock cycles, allowing the 3D segments to be used in a first level trigger system.

The Gas Pixel detectors design (gas composition, drift gap, electronics) depends on the required functionality. For high energy physics application it can be a tracking only device or, filled with Xe-based gas mixture, may also combine tracking and transition radiation detector properties [5]. The detectors aimed to operate close to the interaction point and at high particle density should have a rather thin drift gap (1-2 mm) and use a fast and low diffusion gas mixture (see for instance [7]). If it is aimed to provide also a track segment it should have a drift gap of 5-10 mm and a specially designed front-end electronics to be able to process data at the front-end level. It was shown that with low diffusion gas mixture a spatial resolution of Gas Pixel detectors is approaching 10 μm level [5,7]. Spatial resolution of about 8 μm is reached in [6]. For transition radiation (TR) registration the detector should have significant drift space >20~mm filled with Xe-based gas mixture for effective absorption of TR photons. The read-out electronics in this case should also measure the signal amplitude in each pixel.

The advantage of Gas Pixel detectors as TRD devices is their capability to reconstruct a microscopic picture of ionization on the particle track and, hence, maximize separation between ionization and TR clusters.

Gas Pixel technique is at the beginning of its development but already now it finds applications in different areas, such as: dual-phase noble gas time projection chamber for dark matter search [10], low background single photon detector in the CAST experiment [11], x-ray polarimetry detector for X-ray astronomy [12], etc.

In paper [6] detailed studies of tracking properties of the Gas Pixel detector filled with Ar and DME base mixtures are presented. Figure 2 shows test beam geometry for studies of the chambers (right picture), track projection of the chip plane (middle) and reconstructed track segment in the plane perpendicular to the chip plane. Results shown on this figure obtained with DME/CO2 mixture, which has very low diffusion. Time properties of the TimePix amplifier are quite poor (~100 ns signal rise time). This significantly affects an accuracy of the measured distance form the ionization cluster to the chip plane.

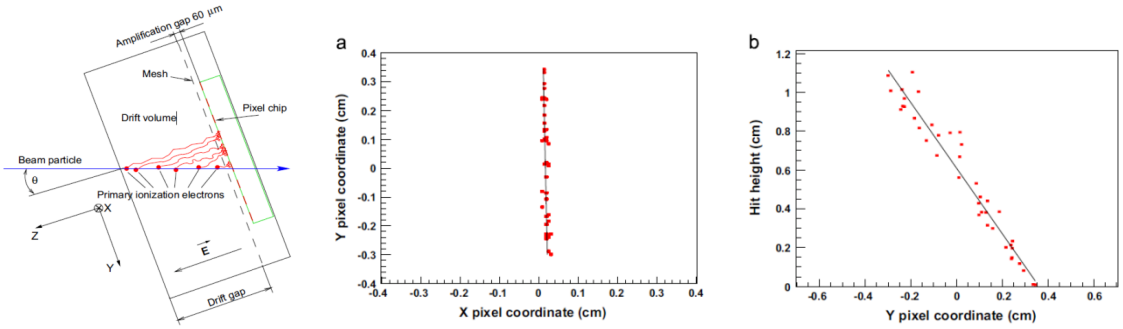

Figure 2. Test beam geometry for studies of the Gas Pix detector (right), track projection of the chip plane (middle) and reconstructed track segment in the plane perpendicular to the chip plane[6].

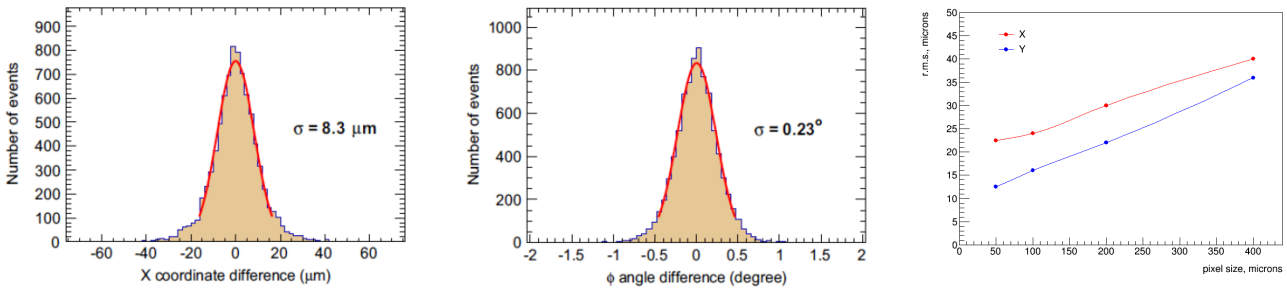

Figure 3. DME- based mixture. Particle impact parameter measurement accuracy across the track projection (left) and angle measurement accuracy (middle) of the tack projection on the chip plane. Solid lines represent Gaussian fits applied to the central parts of distributions. Right picture shows particle impact parameter measurement accuracy as a function of the pixel size.[6].

Some plots demonstrating performance of this detector with DME/CO2 mixture are shown in Fig. 3. Particle impact parameter measurement accuracy across the track projection is shown on right picture.

The middle picture shows angle measurement accuracy of the tack projection on the chip plane. Solid lines represent Gaussian fits applied to the central parts of distributions. Right picture shows particle impact parameter measurement accuracy as a function of the pixel size. One sees that excellent track segment reconstruction properties are obtained in the pixel plane. Space accuracy depends on the pixel size and deteriorates from ~10 μm to 20 μm when pixel size is changed from 50 to 200 μm.

In Ar-based mixture diffusion is large and number of ionization clusters is less. This leads to a decrease of the track segment measurement accuracy. Figure 4 shows the particle impact parameter measurement accuracy across the track projection as a function of pixel size (left) and as a function of particle incident angle (middle). Angle measurement accuracy of the tack projection on the chip plane as a function of incident angle shown of right picture.

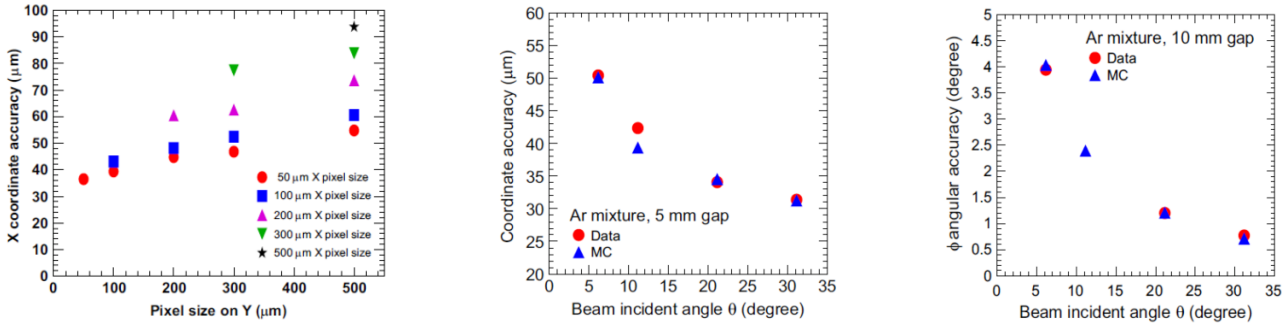

Figure 4. Ar-based mixture. Particle impact parameter measurement accuracy across the track projection as a function of pixel size (left) and as a function of particle incident angle (middle). Angle measurement accuracy of the tack projection on the chip plane as a function of incident angle (right) [6].

It is clear from these figures that even with Ar- mixture one obtains very good tracking properties of the Gas Pixel detectors. However these results are based on offline analysis which uses all available information from the detector. It is clear that for fast processing at the front-end level the analysis should use other algorithms, which can be implemented directly in the read-out chip. Next Section describes these algorithms and shows how they results in the performance of the detector.

2. Online track reconstruction algorithms in Gas Pixel Detectors

It is assumed that the algorithms can be realized on hardware level within the chip electronics [13]. As an example the LHC clock parameters for chip operation were used (40 MHz, or 25 ns time bin) for simulations. This frequency is used inside the chip electronics to collect, analyze and transmit the data. It is assumed that signal shaping is fast enough to fit 25 ns time bin. For demonstration next chamber parameters were chosen: drift gap 10 mm, maximum drift time 200 ns, pixel size X=200 μm, Y=100 μm. Chamber filed with Ar-mixture.

As it was already mentioned electrons generated by an ionizing particle in a gas drift along Z axis perpendicular to the chip surface (XY plane) independently of the particle trajectory. Schematically a

model of this chamber used in simulation is presented in Fig. 5. On this figure XZ projection of the particle track is shown. The Z axis has two scales: one is the distance from the ionization cluster to the chip plane (0-10 mm), and the second one is the corresponding drift time (0-200 ns). The track angle to Z axis in this projection is θ.

Let's suppose that the particle crosses the detector at the time $t_0 = 0$. The electrons produced close to the cathode will drift to anode in the maximum time and arrive there at t = 200 ns. But for electrons generated very close to the grid the drift time will be close to zero. Thus during the 200 ns period all the electrons generated by the particle will be collected and registered on the chip.

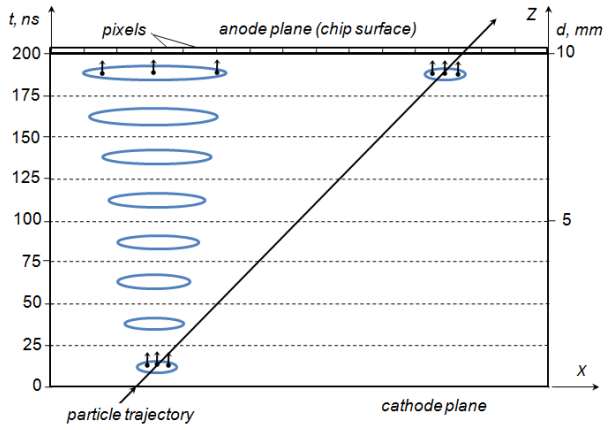

Figure 5. Cross section of GPD with the particle trajectory projection.

For the readout cycle of 25 ns, all the available information related to the particle trajectory will be received in 8 cycles. The time scale in Fig. 5 is divided into 8 parts of 25 ns each, what corresponds to 1/8 of 10 mm distance from cathode to anode or 1.25 mm. For the time interval t = 0 - 25 ns, the average drift time 25 / 2 = 12.5 ns corresponds to the particle-to-chip distance 1.25 / 2 = 0.625 mm. The calculated values of X and Y coordinates of the pixels fired during the time interval - n represent the position of the particle in the detector at the third coordinate Z = 0.625 mm + 1.25·(n-1) mm. All this makes possible to reconstruct the particle trajectory.

The process of transverse diffusion spreads the electrons around the particle trajectory during their drift through the gas volume. A few tenths of pixels can be fired for each of 25ns readout cycle. A method of data acquisition and online analysis using averaging technique is proposed to be used. Every pixel has an integrated fast preamplifier, discriminator and flip-flop (FF) with two fixed current outputs connected to common X and Y lines going along the particular X_i and Y_i rows correspondingly (see Fig. 6). If a pixel is fired during a cycle, FF turns ON and current flows along the line. If a few (up to 15) pixels have been fired in the same row in the same readout cycle, the sum of their currents appears in the corresponding line as shown in fig. 7.

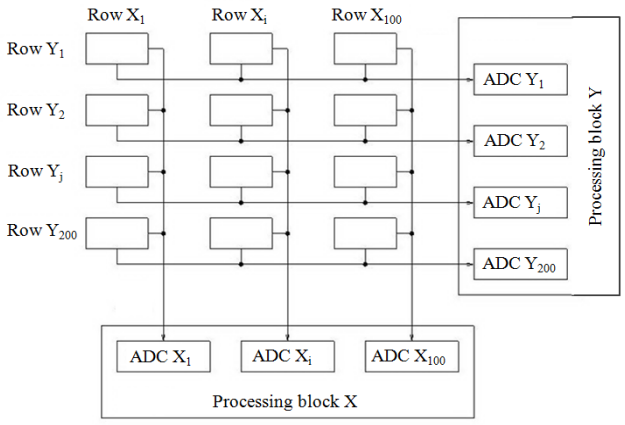

Figure 6. The block diagram of the readout algorithm.

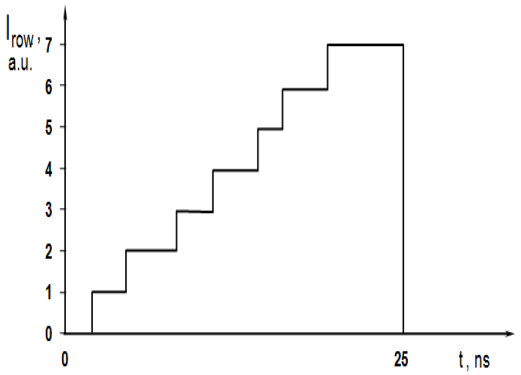

Figure 7. An example of the current in the row line if 7 pixels are fired during one 25ns cycle.

Because all the pixels generate equal currents the sum is linearly proportional to the number or fired pixels. The end of each line is connected to a 4-bit flash ADC integrated in the X and Y processing blocks PBX and PBY positioned on the two edges of the chip. At the end of each cycle a special command is generated and all the ADCs convert the current into the number of fired pixels in this row. The same command returns all the FFs into starting position preparing the channel to next readout cycle. This method allows to transmit the information from the row to the ADC using only one wire.

If particle crossed the detector perpendicularly to the chip plane, both angles θ and φ are zero and the mean position of fired pixels cluster in XY coordinates is the same for all 8 cycles. Only the number of fired pixels increases from 1-st to 8-th cycle because of transverse diffusion. If one or both angles are not zero the clusters move along X and Y with a cycle number reflecting particle trajectory within the detector. Fig.8 illustrates an example of cluster structure in one of the events in XY plane and its projections on both axes for the 3-rd of 8 cycles. In order to calculate particle position in row number units we use a centre of mass approach. In each projection the row number R^i_X and R^j_Y is multiplied by the number of fired pixels in this row n^i_X or n^j_Y ,and the sum of the products is divided by the total number of fired pixels in the cluster N_P:

$$X = \sum R^i_X n^i_X \Big/ N_P \qquad Y = \sum R^j_Y n^j_Y \Big/ N_P$$

This procedure is performed for each of 8 cycles. Cycle number is assigned to the corresponding Z coordinate as described above. Thus we can create two plots representing the XZ and YZ projections of the particle trajectory with 8 sets of found coordinates shown as dots in each plot. An example of one simulated event is presented in Fig. 9, where a straight line is drawn through 8 points using the least-squares method. From there we can determine the particle trajectory, i.e. XY coordinates where the particle crossed the cathode and anode planes as well as both angles: θ in the XZ plane and φ in YZ plane.

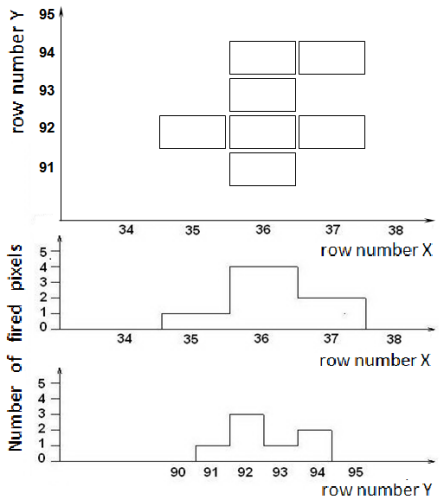

Figure 8. The example of the cluster structure in XY plane and its projections on X and Y axes.

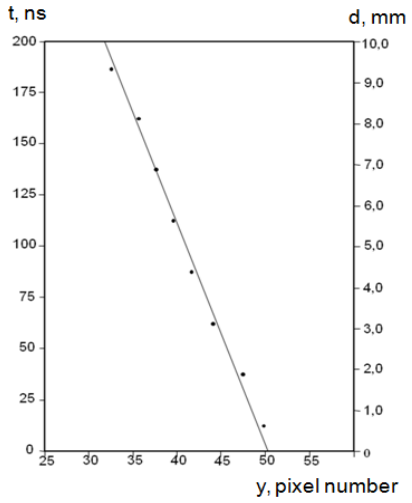

Figure 9. The example of the particle trajectory reconstruction.

In order to estimate an expected resolution, which can be obtained with this method, dedicated MC simulations have been carried out. Fig. 10 shows the example of simulated distributions for the 20 GeV pions crossing the detector with θ = 20°and φ = 3°. It is clearly seen that the average values of the reconstructed angles (θ = 20.06° and φ = 3.00°) is very close to the initial ones, and the r.m.s is about 0.4°. For the reconstructed impact points r.m.s. is 0.26 of pixel size for X and 0.31 for Y coordinates, which corresponds to 52 and 31μm respectively. This numbers are in a very good agreement with ones obtained in the test beam and presented in Section 1.

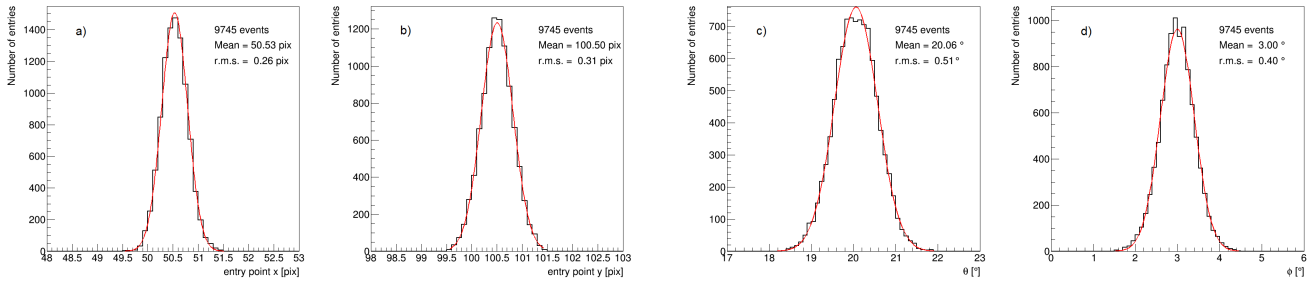

Figure 10. The distributions of the reconstructed track entry points coordinates: a) X; b) Y; and angles: c) θ; d) φ for 20 GeV pions crossing the GPD with θ = 20° and φ = 3.00°.

3. Hybrid Silicon-Gas Pixel Detectors (HSiGPD)

3.1 Preamble

As it was demonstrated there are many advantages of the Gas Pixel detector show ever there are also a few points to be improved. One of them is the measurements of the moment at which particle crossed the detector. In many studies timing precision is a very important parameter. In the scheme

presented above a natural time bin, which is defined timing is 25 ns. There are many effects which timing of the events in this detectors: signal shaping time, ionization cluster distribution and electronics threshold, a time walk due to signal amplitude etc. These affect may stretch time jitter over even 25 ns. In a self-triggering mode this will lead to an assignment of the event to a wrong bunch crossing (in case of LHC). If detector has independent timing device this would significantly improve its performance and application areas. Another issue is operation in a dense particle environment. Fast reaction of the particle crossing detector would allow remove ambiguities arising from particles coming at different time during the operation cycle.

One of the ways to solve problems of correct time measurement is to add a sensitive layer in existing Gas Pixel chip with independent readout. This can be done introducing an epitaxial layer during regular chip production technology [14]. This would allow to make a new type of detector HSiGPD which would keep all the properties of Gas Pixel Detector (PGD) and use additional Si sensitive layer for timing and coordinate measurements. New chip is possible to make in the same production cycle what ensures no significant increase in the production cost. HSiGPD detector should have high timing precision and can be used as a self-triggered device.

3.2 Silicon pixels implementation

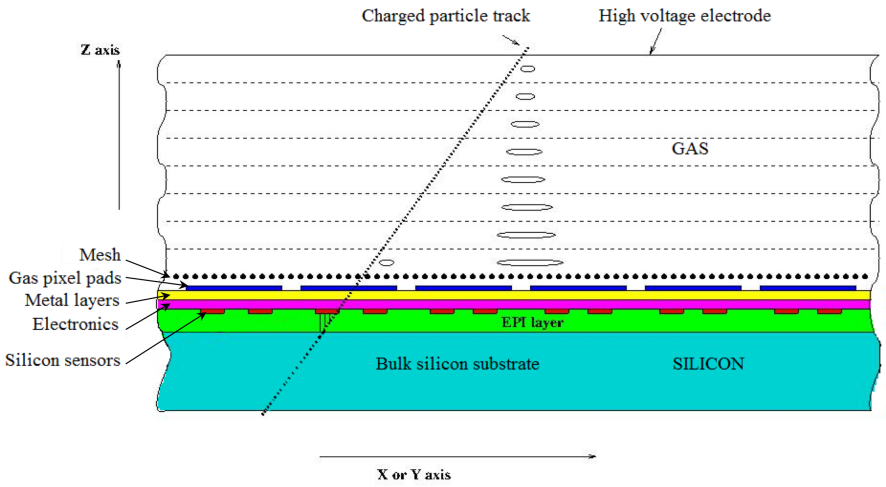

Figure 11. The schematic view of HSiGPD structure.

Schematically, a design of the HSiPGD detector is shown in Fig 10. The basis of the HSiPGD detector can be a Gas Pixel chip which has 100×200 μm pixel size distributed over the 2×2 cm^2 electronic chip surface. Each pixel electronics is positioned under the pixel. Data acquisition and processing electronics is situated at X and Y edges of the chip. Function of this electronics is described on section 2. Under Gas Pixel readout electronics additional layer of pixel electronics connected to 25×25 μm sensors covered by epitaxial Si layer is introduced. Electrons produced by the charged particle in the epitaxial layer are collected on sensors in very short time interval ~1 ns what defines timing properties of the chip. Additional pixel payer readout gives XY coordinate of the particle with 7

μm accuracy. In order to reduce power consumption/dissipation the silicon pixel size can be increased to 50×50 μm which would lead to15 μm coordinate accuracy.

Each chip has supplied with external or internal clock and develops own trigger. It starts the readout process when particle crosses detector volume. Chip generates as many cycles as needed to collect and analyze the data from the pixels and transmit the information about particle coordinates and both angles. For collider experiments HSiGPD the external clock is synchronized with beam crossings. External clock of 40 MHz can be used as a basis to increase internal clock frequency up to 80, 120 or 160 MHz. This will increase the speed of data processing in FE electronics.

Chip electronics for Si sensors operates similar way as for the Gas Pixel detector. It analyses the data and measures both X and Y coordinates. Combination of information from both detectors would allow reconstruct track segment with associated tame stamp at FE level. The latency of output information could fit to 40 clock periods what gives 1 μs for 40 MHz clock frequency. 80 MHz clock frequency would give of about 0.5 μs latency. 80 MHz looks as a very realistic clock speed even for 0.25 μm chip technology.

4. HSiGPD chip electronics blocks

4.1 HSiGPD chip layout

General layout of the HSiGPD readout chip is presented in Fig. 12. GPD chip electronics consists of blocks under each gas pixel pad, peripheral processing blocks (X-coordinate processing and Y-coordinate processing blocks) and some communication logic to transfer data to host computer.

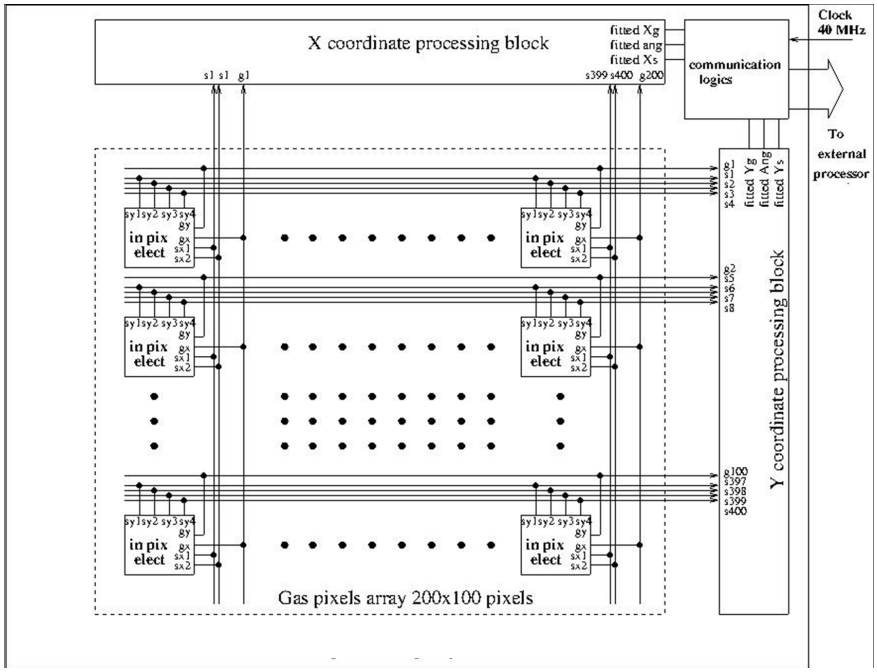

Figure 12. HiGPD chip layout.

One chip contains 200 x 100 pixels covering area 2 x 2 cm^2. Si sensor read out has the same layout and situated under GPD read out. A proposed size of gas pixel pads is $100\times200\mu m^2$, while for silicon sensors pixel size is 25×25 μm^2or 50×50 μm^2. In that case "in pixel electronics" element of the readout will contain1 block of gas pixel detector and 32 or 8 blocks of silicon detector. All signals from the pixels in 1 row are combined on 1 wire, making the row of pixels similar to strip in micro-strip detector, and the same is done for each column. Thus, each pixel generates 2 outputs– one for "X-strip" another for "Y-strip". Same procedure is employed for silicon sensor outputs, with some difference, though. For gas pixels each pixel contributes fixed amount of current into the row wire and total current reflects how many pixels in the given strip had generated signal. We are not doing this for silicon sensors – every strip has the logical OR of all signals are generated.

4.2 In-pixel electronics

Fig.13 shows the block diagram of the electronics under each gas pad–"in pixel electronics". As it was noticed earlier, there is 1 block for gas pad and 8 or 32 blocks for silicon sensor. The "offset" is set to create some threshold for comparator firing, to exclude firing from noise and cross-talks. In order to obtain information for each time bin the gas part chip requires a reset signal after each sampling interval. This is done connecting the pad to fixed offset voltage what removes all charge accumulated earlier. This can be very short signal – just few ns. It may be a challenge to provide such short signal distributed through all chip area. "Bias" input is used to adjust value of the current output provided to current summing wires.

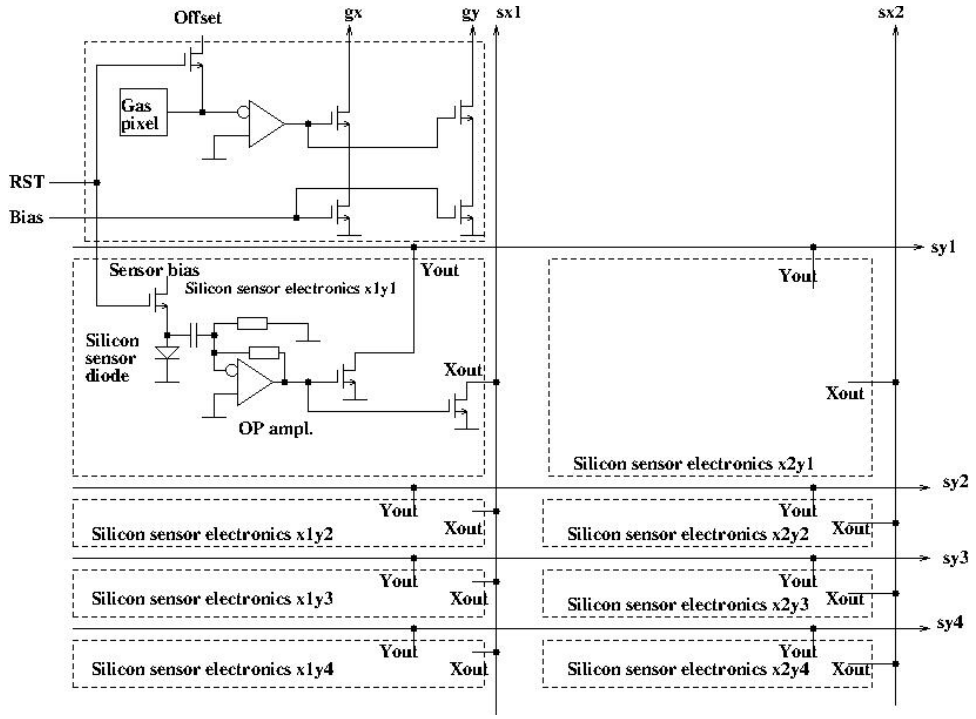

Figure 13. In-pixel electronics.

For the silicon signal sensor there is another challenge. Because signal value is comparable to possible spread of the input transistor parameters, we can't make it DC coupled to the signal. AC coupling is suggested to be used in that case.

4.3 Coordinate processing block

A coordinate processing block is shown in fig. 14. It is similar for X- and Y-coordinates, difference is only in the number of inputs from gas pixels.

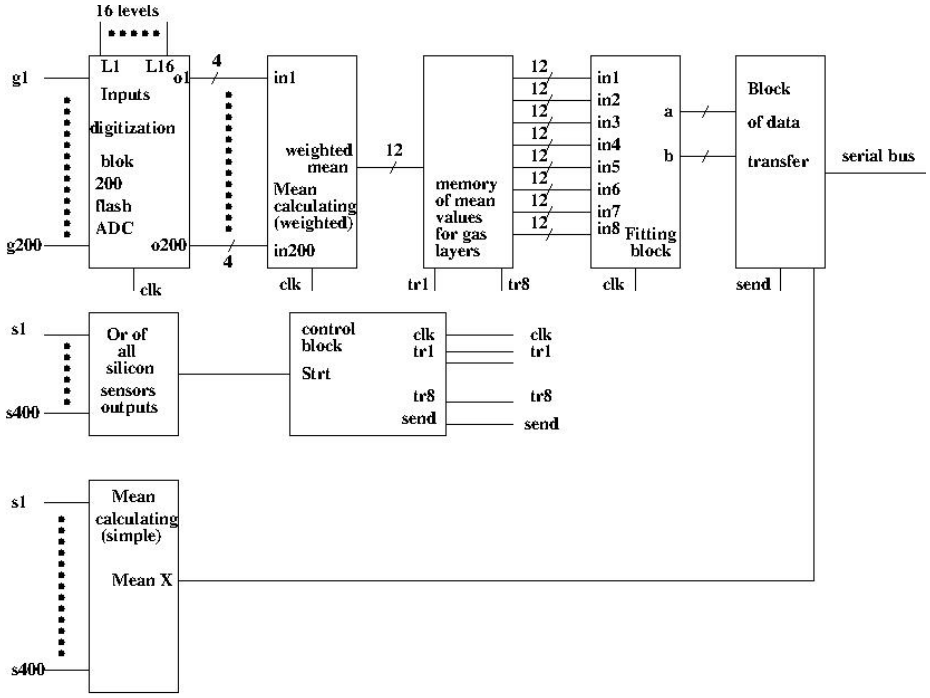

Figure 14. Coordinate processing block.

These blocks are located in the area at the ends of X or Y strips. It is pretty large area, having about 2 cm in length and few mm in width. So, big number of electronic elements can be placed here.

The input digitization block consists of 200 (or 100) flash ADC. ADCs must digitize signals coming every clock (for 8 subsequent clocks). Each flash ADC has a shorter pipe line to allow make a few digitization steps such as: sample and hold, comparison to fixed levels, digitization of the results of comparison. This all can be matched to 3-4 clock period latency. With this delay the results will be delivered each clock cycle.

In Fig.15 a block diagram of the "Weighted mean" component is presented. Outputs from flash ADC are proportional to a number of hits in the given strip of pixels. To calculate average coordinate we need to multiply each coordinate by number of hits at this coordinate and divide it by total number of hits.

Flash ADC generate 4 bits values (should be enough, if number of fired hits in one strip does not exceed 15). 5 bits ADCs can also be an option if needed, but this will be a bit more difficult, as it requires higher precision in thresholds comparisons. To do multiplication of ADC output by constants, representing strip coordinates (1,2,3,4 …) we suggest the use of look up tables (LUTs) made of ROMs (Read Only Memory). For 16 bit input address they are small enough (16 memory cells each).

Outputs of LUTs are fed to 200 input adder for calculating sum of weighted coordinates, while another 200 inputs adder calculates the sum of weights (number of hits). The sum of weighted coordinates may have maximum value of 157500 (if all 200 strips had 15 hits each). Such number can be represented by 18 bits binary. It is the nominator for divider block. Denominator is the sum of weights, maximum value is 10500, and it can be 14 bits number. It is used as denominator in divider.

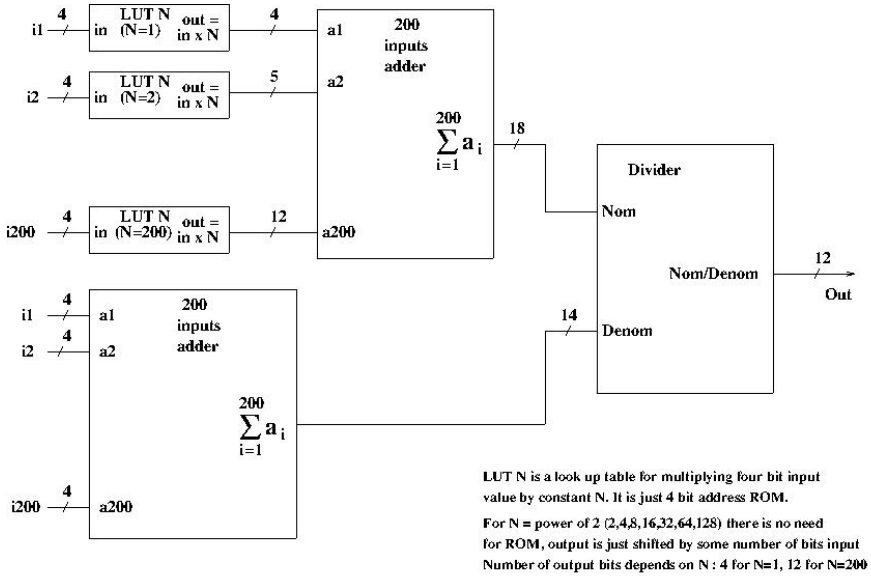

Figure 15. Weighted mean calculating block.

The divider output precision can be select according to needs. If we have maximum coordinate 200 strip widths and want to have precisions of 1/16 strip, we need to encode maximum value of 3200, and for this we need 12 bits. Selecting 12 bits for divider output we are setting number of clocks for divider to complete division to 12.

The adder block is shown in fig.16. This is a cascade of 2 inputs adders, and we need 8 levels to calculate the sum. Total number of 2 input adders will be 199.

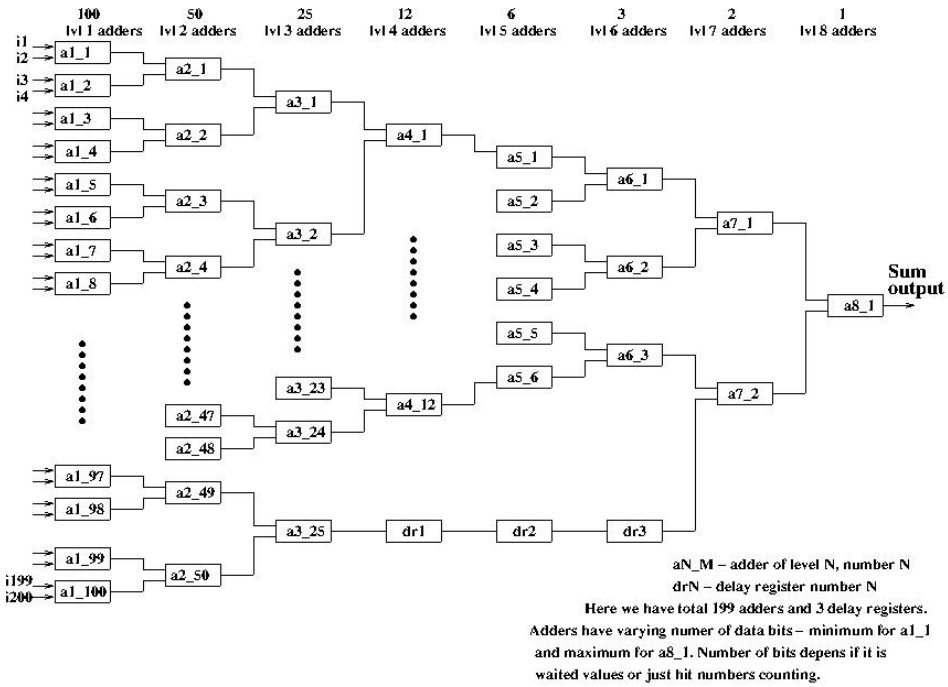

Figure 16. 200 inputs adder block.

As at some level number of adders may became odd, we need to propagate to next level even number of outputs, and remember leftover one for adding at some later level, when again odd number of outputs from previous level appear. To have it coming synchronously with other terms, we need to delay this value by proper number of clocks.

Simple mean calculation block is done the same way as weighted mean, but without using LUTs as all weights are 1.

The next block is a memory of mean values for gas layers. We need to store 8 coordinates, corresponding to 8 gas layers to fit the track. These values are appearing on the weighted mean calculating blocks in 8 consecutive clocks after some delay related to all previous processing steps. The synchronization pulses to save values are generated by control block. The same control block generates the clocks for fitting after all 8 values are saved.

Fitting block is shown in fig.17. Fitting of the formula y=az+b (or x=az+b) is done using minimum squares method. The formula for calculating angle coefficient a is shown on the figure. For level 1 trigger we need only the angle.

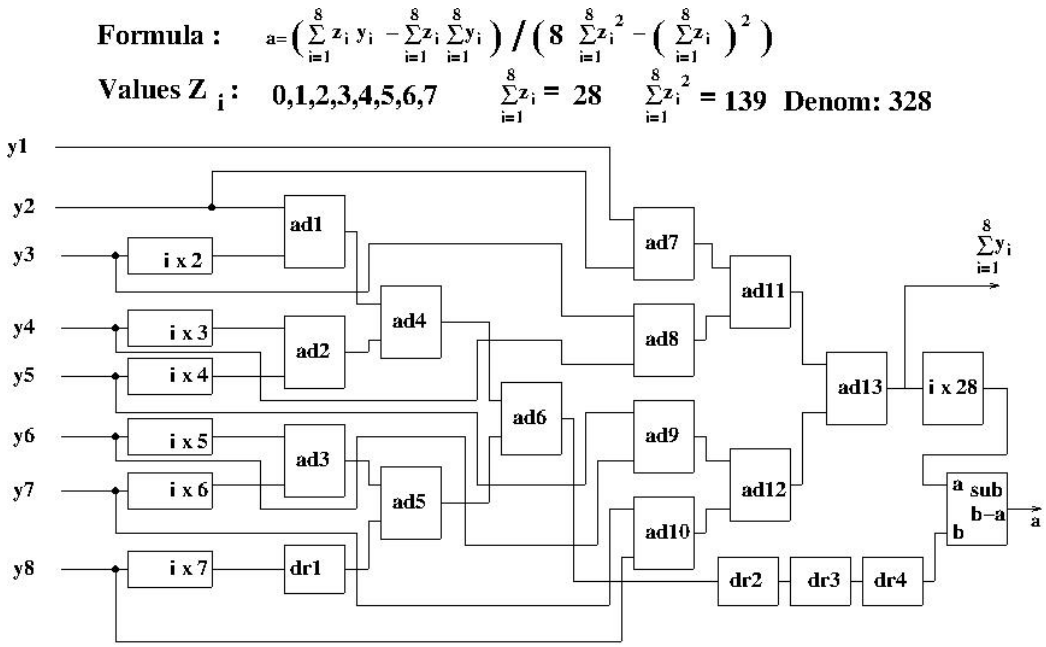

Figure 17. Fitting block.

For fitted coordinate we need to subtract the sum of z coordinates multiplied by this angle coefficient from the sum of y coordinates (for 8 points). The multiplication requires more time, so we may not want to do it on the chip, but transmit the coefficient and some of y values to external processor. For generating level 1 trigger we need to compare angle with some threshold, it can be done in 1 clock. So, the total latency of the level 1 trigger signal, if we add together all latencies discussed earlier, will be 43 clocks.

5. Conclusions

Combination of the GPD with thin active layer of Si integrated within electronics readout chip allows to produce a new type of detectors - HSiGPD with significantly extend functionality. These type of detectors at low material budget and relatively cheap structure would have self-trigger mode of operation with a good coordinate and an angular accuracies of particle track segment reconstruction. Self-trigger functionality would allow to extend application of such detector systems beyond high energy physics filed. New detectors will have fast on-line data processing functionality and ability to provide charged particle trajectory measurements within ~0.5 μs. This gives a possibility to use them as a first level track trigger system. One should not that a technology of Si-detector production which is a part of the proposed hybrid detector goes alone with the HVCMOS detector technology which is extensively developed now [15].

Bibliography

1. R. Bellazzini, et al., Nucl. Instr. and Meth. A 535 (2004) 477.
2. M. Chefdeville, et al., Nucl. Instr. and Meth. A 556 (2006) 490.
3. V. Blanco Carballo, et al., Journal of Instrumentation 5 (2010) 02002.
4. V. Blanco Carballo, et al., Nucl. Instr. and Meth. A 629 (2011) 118.
5. F. Hartjes, et al., Nucl. Instr. and Meth. A 706 (2013) 59.
6. A. Boldyrev, et al., Nucl. Instr. and Meth. A807 (2016) 47–55.
7. W.J.C. Koppert, et al., Nucl. Instr. Meth. A 732 (2013) 245.
8. K.A. Olive, et al., (Particle Data Group), Chin. Phys. C, 38, 090001 (2014), chapter ``Micro-Pattern Gas Detectors".
9. K.A. Olive, et al., (Particle Data Group), Chin. Phys. C, 38, 090001 (2014), chapter ``Time Projection Chamber".
10. R. Schon, et al., Nucl. Instr. and Meth. A 718 (2013) 446.
11. J. Kaminski, et al., Journal of Physics: Conference Series 460 (2013) 012004.
12. R. Bellazzini, et al., Nucl. Instr. and Meth. A 579 (2007) 853.
13. N. Sinev, et al., Journal of Physics: Conference Series, vol. 675 (2015) 012021.
14. G. Bashindzhagyan, et al., will be published in Journal of Physics: Conference Series (2016).
15. I. Perić et al., JINST, 2017, 12 C02030